# Synthesis, and Characterization and In-Silico Analysis Against SARS CoV-2 of Novel Benzimidazolium Salts

Elvan Üstün * [iD] [a], and Neslihan Şahin [iD] [b]

N-heterocyclic carbene molecules are often used as the main scaffold in pharmaceutical chemistry, and one of the most important of these is benzimidazoles. Severe Acute Respiratory Syndrome Coronavirus Disease-2 is the cause of the ongoing pandemic, and a drug should be developed against this virus. Scientists have been investigated the antiviral effects of many not only known molecules but also new molecules. In this study, reactivity and anti-coronavirus disease properties of new benzimidazole derivative molecules were investigated by theoretical methods. Three new benzimidazole derivative molecules were synthesized and fully characterized by FT-IR, ^{1}H NMR and, ^{13}C{^{1}H} NMR spectroscopies for this purpose. Density Functional Theory-based calculation methods were used for optimization and frontier orbitals analysis. Also, the interactions of the molecules were evaluated with coronavirus disease main protease, and severe acute respiratory syndrome coronavirus main peptidase and the results were compared with the results of well-known anti-viral drugs by molecular docking methods. According to the results, 1-allyl-3-(3-chlorobenzyl-5,6-dimethylbenzimidazolium chloride represent the best result against both main protease and main peptidase enzyme with -6.36 kcal/mol and -8.87 kcal/mol, respectively. Additionally, three of the molecules were give better binding results than the well-known anti-viral drugs.

Graphical abstract
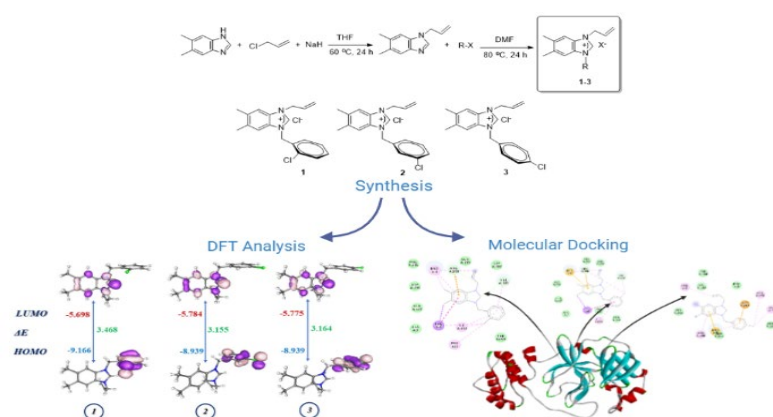
1. Introduction

N-Heterocyclic Carbene (NHC) is one of the most frequently studied families due to their strong sigma-donor and weak pi-acceptor properties during metal bonding [1, 2]. Since the synthesis and isolation of the first NHC by Arduengo in 1991, NHCs and their metal complexes have been used for many industrial and pharmaceutical purposes [3-5].

Heterocyclic azoles such as imidazole, triazole and especially benzimidazole are remarkable molecules since their biological activities [6]. The benzimidazole scaffold is a useful main motif for development of biological and pharmaceutical active molecule [7]. Substituted benzimidazole derivatives are well-known with their antihistaminic, anticancer, antifungal,

a Department of Chemistry, Faculty of Art and Science, Ordu University, 52200, Ordu, Turkey. **b** Department of Science Education, Faculty of Education, Cumhuriyet University, 58140, Sivas, Turkey. *Corresponding author. E-mail: **elvanustun77@gmail.com**

antiviral, antihypertensive and antiulcer [8, 9]. Omeprazole (proton pump inhibitor), pimobendan (inotropic), and mebendazole (anthelmintic) could be recorded as benzimidazole type drugs [10, 11]. Benzimidazole derivative molecules with pharmacological properties have also been reviewed by many authors [12-14].

Severe Acute Respiratory Syndrome Coronavirus Disease-2 (SARS CoV-2) still continues as the biggest pandemic that this generation has ever seen. According to the data of the World Health Organization [24.10.2022], 624.235.272 confirmed cases of Coronavirus Disease-19 (COVID-19), including 6.555.270 deaths were recorded [15]. The fight against the pandemic continues by vaccination. Since temporary effects and worldwide availability of vaccination, an anti-viral drug must be discovered for a real victory against the pandemic [16, 17]. Several drugs which are effective against other analogues viruses are already used for the treatment of patients [18, 19]. Scientists have been tested the anti-viral properties of both newly synthesized and many known molecules [20-22]. However, considering the budget, and the laboratory possibilities and the urgency of circumstances, it is not possible to try all possible natural and synthetic molecules.

The developments in theoretical chemistry researches in recent years are noteworthy [23, 24]. Since the compatibility of the calculated values with the experimental results, it is possible to obtain useful information about the molecules before the synthesis. In addition, functional data about the reactivities of the molecules can be obtained by using the orbital energies [25, 26]. Moreover, the interaction details between the molecules and effective biological macromolecules can be investigated by molecular docking methods. In this study, 1-allyl-3-(2-chlorobenzyl-5,6-dimethylbenzimidazolium chloride (**1**), 1-allyl-3-(3-chlorobenzyl-5,6-dimethylbenzimidazolium chloride (**2**), and 1-allyl-3-(4-chlorobenzyl-5,6-dimethylbenzimidazolium chloride (**3**) were synthesized and fully characterized by FT-IR, ^{1}H NMR and, ^{13}C{^{1}H} NMR spectroscopies. Density Functional Theory (DFT)-based calculation methods were used for optimization of their structures with exchange functional BP86 with TZV basis set. HOMO (Highest Occupied Molecular Orbital) and LUMO (Lowest Unoccupied Molecular Orbital) were analyzed, and Global Reactivity Descriptors of the molecules were carried out by Koopmans Theorem. Also, the interactions of the molecules were evaluated with COVID-19 main protease (pdb id: 5r82), and SARS coronavirus main peptidase (pdb id: 2gtb) and the results were compared with the results of well-known anti-viral (favipiravir, hydroxychloroquine, lopinavir, nelfinavir, remdesivir) by molecular docking methods.

2. Material and Methods

All molecules were achieved by using Schlenk techniques in flame-dried glassware under argon and all the solvents were purified over the suitable drying agent and transferred under Argon. All reagents were purchased from Sigma Aldrich Co. (Dorset, UK). Electrothermal 9100 were used for determination the melting points of the molecules in capillary tubes. Perkin Elmer Spectrum 100 FT-IR were used for Fourier transform infrared spectra and also Bruker As 400 Mercury spectrometer operating at 400 MHz (^{1}H), 100 MHz (^{13}C) in CDCl$_3$ were used for ^{1}H NMR and ^{13}C{^{1}H} NMR spectra with tetramethylsilane as the internal reference.

2.1 General procedure for the preparation of N-heterocyclic carbene salts

Benzimidazolium salts (**1-3**) were synthesized according to the literature [27].

1-Allyl-3-(2-chlorobenzyl-5,6-dimethylbenzimidazolium chloride, 1

5,6-dimethylbenzimidazole (10 mmol) was added to a stirring solution of NaH (11 mmol) in tetrahydrofuran (20 mL). After the solution was stirred at room temperature (RT) for 1 hour, allyl bromide (10.1 mmol) was added to the solution which was stirred at 60 °C for 24 hours. Before the solvent was evaporated in vacuo, the solution was cooled to the RT. The latter solution was distilled from 30 mL dichloromethane and 1-allyl-5,6-dimethylbenzimidazole was achieved. 1-allyl-5,6-dimethylbenzimidazole (1 mmol) and 2-chlorobenzyl chloride (1 mmol) were stirred in dimethyl formamide (DMF) (5 mL) for 24 h at 80 °C and precipitated product was cleaned by diethyl ether and dried under vacuum. Yield: 78%; m.p. 209-210 °C, FT-IR $\nu_{(CN)}$: 1553 cm^{-1}. ^{1}H NMR (400 MHz, CDCl$_3$) δ (ppm): 2.38 (t, 6H, NC$_6$H$_2$N(CH_3)$_2$-5,6, *J* = 14 Hz), 5.27-531, 5.37-5.46 (m, 4H, NCH_2CHCH_2), 5.93 (d, 2H, CH_2C$_6$H$_4$-Cl-2, *J* = 16 Hz), 6.09 (quint, 1H, NCH$_2$CHCH$_2$, *J*= 4 Hz), 7.27-7.58 (m, 6H, Ar-*H*), 11.60 (s, 1H, NC*H*N). ^{13}C{^{1}H} NMR (100 MHz, CDCl$_3$) δ (ppm): 20.7 (NC$_6$H$_2$N(*C*H$_3$)$_2$-5,6), 48.4 (*C*H$_2$C$_6$H$_4$-Cl-2), 50.0 (N*C*H$_2$CHCH$_2$), 128.1 (NCH$_2$CH*C*H$_2$), 133.5 (NCH$_2$*C*HCH$_2$), 113.3, 121.3, 129.9, 130.1, 130.5, 130.7, 130.8, 137.4, 137.5 (Ar-*C*), 143.1 (N*C*HN).

1-Allyl-3-(3-chlorobenzyl-5,6-dimethylbenzimidazolium chloride, 2

2 was obtained with the same procedures as described for **1**. However, 3-chlorobenzyl chloride (1 mmol) was used as alkyl halide. Yield: 76%; m.p. 215-216 °C, FT-IR $\nu_{(CN)}$: 1555 cm^{-1}. ^{1}H NMR (400 MHz, CDCl$_3$) δ (ppm): 2.39, 2.41 (s, 6H, NC$_6$H$_2$N(CH_3)$_2$-5,6), 5.23 (d, 2H, NCH_2CHCH$_2$, *J*= 4 Hz), 5.44-5.48 (m, 2H, NCH$_2$CHCH_2), 5.91 (s, 2H, CH_2C$_6$H$_4$-Cl-3), 6.11 (quint, 1H, NCH$_2$CHCH$_2$, *J*= 4 Hz), 7.30-7.32 (m, 3H, Ar-*H*), 7.41-7.46 (m, 3H, Ar-*H*), 11.78 (s, 1H, NC*H*N). ^{13}C{^{1}H} NMR (100 MHz, CDCl$_3$) δ (ppm): 20.7 (NC$_6$H$_2$N(*C*H$_3$)$_2$-5,6), 50.1 (*C*H$_2$C$_6$H$_4$-Cl-3), 50.4 (N*C*H$_2$CHCH$_2$), 126.5 (NCH$_2$CH*C*H$_2$), 135.0 (NCH$_2$*C*HCH$_2$), 113.2, 113.3, 121.7, 126.5, 127.8, 129.3, 129.6, 129.7, 129.9, 137.6, 137.7 (Ar-*C*), 142.6 (N*C*HN).

1-Allyl-3-(4-chlorobenzyl-5,6-dimethylbenzimidazolium chloride, 3

3 was obtained with the same procedures as described for **1**. However, 4-chlorobenzyl chloride (1 mmol) was used as alkyl halide. Yield: 79%; m.p. 218-219 °C, FT-IR $\nu_{(CN)}$: 1561cm^{-1}. ^{1}H NMR (400 MHz, CDCl$_3$) δ (ppm): 2.39, 2.41 (s, 6H, NC$_6$H$_2$N(CH_3)$_2$-5,6), 5.22 (d, 2H, NCH_2CHCH$_2$, *J*= 4 Hz), 5.41-5.46 (m, 2H, NCH$_2$CHCH_2), 5.88 (s, 2H, CH_2C$_6$H$_4$-Cl-4), 6.08 (quint, 1H, NCH$_2$CHCH$_2$, *J*= 4 Hz), 7.30-7.33 (m, 2H, Ar-*H*), 7.35 (s, 1H, Ar-*H*), 7.41 (s, 1H, Ar-*H*), 7.50 (s, 1H, Ar-*H*), 7.51 (s, 1H, Ar-*H*), 11.74 (s, 1H, NC*H*N). ^{13}C{^{1}H} NMR (100 MHz, CDCl$_3$) δ (ppm): 20.7 (NC$_6$H$_2$N(*C*H$_3$)$_2$-5,6), 50.0 (*C*H$_2$C$_6$H$_4$-Cl-4), 50.4 (N*C*H$_2$CHCH$_2$), 131.7 (NCH$_2$CH*C*H$_2$), 135.1 (NCH$_2$*C*HCH$_2$), 113.3, 121.6, 129.5, 129.6, 129.7, 129.8, 137.5, 137.6 (Ar-*C*), 142.5 (N*C*HN).

2.2 Calculation methods

Full unconstrained geometry optimizations with DFT-based calculation methods were carried out with ORCA version 2.8 [28, 29] using the exchange functional according to BP86 that the correlation functional suggested by Becke and Perdew [30, 31], with the resolution-of-the-identity (RI)

approximation, the tightscf and grid4 options, a TZV basis set [32]. Scalar relativistic effects were treated using the Zeroth Order Regular Approximation (ZORA) formalism [33]. To speed up the calculations TZV/J auxiliary basis set was used.

All the global chemical reactivity descriptors were calculated with Koopmans Theorem according to following equations [34, 35]:

$$IP = -E_{HOMO} \tag{1}$$

$$EA = -E_{LUMO} \tag{2}$$

$$\chi = -\frac{I + A}{2} \tag{3}$$

$$\eta = \frac{I - A}{2} \tag{4}$$

$$S = \frac{1}{2\eta} \tag{5}$$

$$\omega = \frac{\mu^2}{2\eta} \tag{6}$$

AutoDockTools 4.2 [36] were used for molecular docking calculations with crystal structure from RCSB protein data bank (pdb id: 2gtb, 5r82) [37, 38]. Only polar hydrogens and Kollman charges were evaluated in target molecules and the waters in proteins were removed. Randomized starting positions, Gasteiger charges, torsions have been evaluated for ligand molecules. While Lamarkian genetic algorithms were applied, the genetic algorithm population was recorded as 150 [39]. Discovery Studio 4.1.0 were used for illustrations [40].

3. Results and Discussion

3.1 Characterization of N-heterocyclic carbene salts

NHC salts (**1-3**) were synthesized as shown Scheme 1. NHC salts (**1-3**) were synthesized by reaction of 1-allyl-5,6-dimethylbenzimidazole 2-chlorobenzyl chloride, 3-chlorobenzyl chloride and 4-chlorobenzyl chloride in DMF at 80 °C, respectively. Precipitated product was crystallized in dichloromethane/diethyl ether for purification. The structure of all new compounds characterized by FT-IR, ^{1}H NMR and, ^{13}C{^{1}H} NMR spectroscopy.
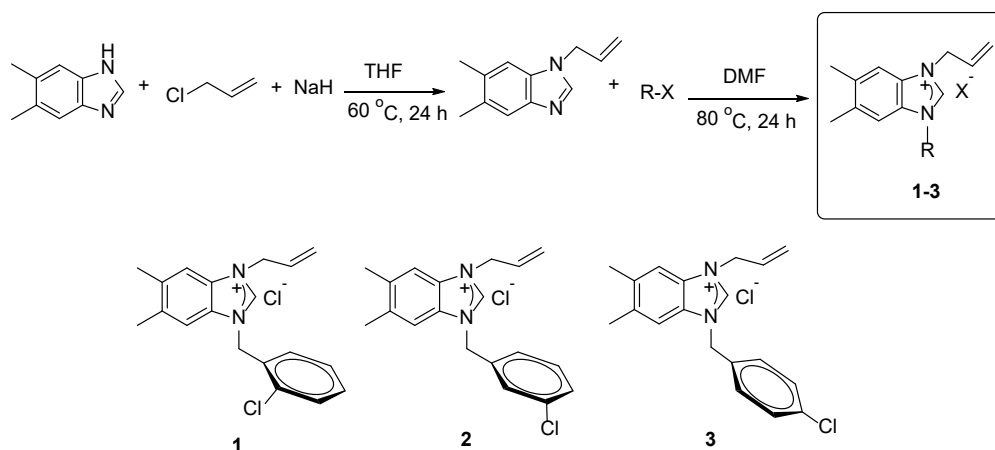
Scheme 1. Synthesis of N-heterocyclic carbene salts (**1-3**).

When the IR spectra of the NHC salts were analyzed, it was observed that the all C-H stretching vibrational bands peaked between 2700-3100 cm^{-1}. C=C stretching vibration modes were assigned at around 1800-1600 cm^{-1}. Benzimidazole ring C=N vibrations of the NHC salts were seen at 1553, 1555, and 1561 cm^{-1} for **1-3**, respectively.

NMR spectra of all the compounds were analyzed in d-CDCl$_3$. In the ^{1}H NMR spectra, acidic protons (NC*H*N) for N-heterocyclic carbene salts (**1-3**) were seen as a sharp singlet at 11.60, 11.78 and 11.74 ppm respectively. Methyl protons in NHC salts peaked around 2.34-2.41 ppm. Benzylic protons of NHC salts (**1-3**) gave peaks 5.93, 5.91 and 5.88 ppm, respectively. Protons of NCH$_2$C*H*CH$_2$ of compounds (**1-3**) came at 6.09, 6.11 and 6.08 ppm as a quint, respectively. In the ^{13}C{^{1}H} NMR spectra, aromatic carbons of compounds **1-3** were seen in the range of 113.0-140.0 ppm. NC*H*N carbon of salts **1-3** were detected at 143.1, 142.6 and 142.5 ppm, respectively. Benzylic carbons of NHC salts gave peak at 48.4, 50.1 and 50.0 ppm for **1-3**, respectively. All methyl carbon peaks of salts were observed at 20.7 ppm for. These values agree with reported data for similar N-heterocyclic carbenes [27]. The FT-IR, ^{1}H NMR, and ^{13}C{^{1}H} NMR spectra are presented in the details in the Supplementary Files (Figures S1, S6).
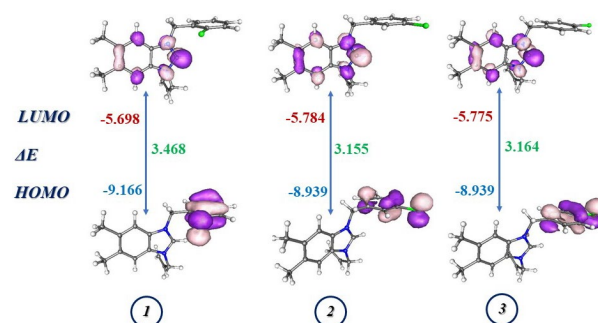
Fig. 1. HOMO and LUMO energies and illustrations of the molecules (in eV).

Structural analysis of coordination complexes gives useful information about the reactivity of molecules [41]. While HOMO provides predictions about the electron donating affinity and region of the molecule, LUMO gives similar information about the electron accepting of the molecule [42]. In this study, relative energy, and region analysis of the frontier orbitals of three benzimidazole derivative molecules were performed by using the same basis sets. In all molecules,

HOMOs are located in the benzyl region, while LUMOs are displayed on benzimidazole. Although the orientation of the HOMOs are different from each other due to substituted chlorine, all the molecules behave as Lewis bases through the benzyl region. Furthermore, according to the HOMO and LUMO energies of the molecules, **1** could be relatively more active in chemical reactions. The energy gap of HOMO-LUMO was calculated as 3.468 eV for 1, and HOMO → LUMO excitation would be relatively more difficult for **1** (Figure 1).

Global Reactivity Descriptors which are calculated according to Koopmans Theory by using the relative energies of frontier molecular orbitals, gives opportunity to make comparisons about the relative reactivity of molecules [43]. Ionization potential, electron affinity and electronegativity are calculated depending on the HOMO-LUMO gap values of the molecules. In addition, chemical hardness and softness provide information on the stability of a molecules in a reaction. The softer molecule is considered as the more unstable and must be the more reactive. Furthermore, the electrophilicity index allows to make comparison the response of a molecule to a nucleophile [44]. It is concluded that **1** is more reactive depending on the ionization potential, electronegativity, and global hardness values according to the calculations in this study. On the other hand, based on the electrophilicity index phenomenon, **1** behaves more efficient against a nucleophile (Table 1).

Table 1. Global reactivity descriptors of the complexes (in eV).

	1	2	3
Ionization Potential (IP)	9.166	8.939	8.939
Electron Affinity (EA)	5.698	5.784	5.775
Electronegativity (χ)	7.432	7.361	7.357
Global Softness (S)	0.288	0.317	0.316
Global Hardness (η)	1.734	1.577	1.582
Electrophilicity Index(ω)	15.908	17.176	17.104

Table 2. Active site analysis of SARS coronavirus main peptidase (pdb id:2gtb) and COVID-19 main protease (pdb id:5r82) with **1**, **2**, **3**, **favipiravir**, **hydroxychloroquine**, **lopinavir**, **nelfinavir**, **remdesivir** (red: H-bond, purple: pi-sigma, blue: Van der Waals interactions, pink: pi-alkyl, green: pi-pi Stacked and pi-pi T-shaped, yellow: pi-sulfur/pi-anion-cation).

Molecule	Bind. Aff.*	Amino Acids Residue
		2gtb
1	-6.25	Gln110, Thr292, Phe294, Leu202, Ile249, Pro252, Pro293, Gly109, Thr111, Ile200, Asn203, Val297
2	-6.36	Gln110, Asn203, Phe294, Ile200, Leu202, His246, Gln107, Pro108, Gly109, Thr111, Glu240, Ile249, Thr292, Pro293
3	-6.16	Gln110, Asn203, Thr292, Leu202, Phe294, His246, Gln107, Pro108, Gly109, Thr111, Ile200, Ile249, Pro293
favipiravir	-3.66	Thr111, Asn151, Thr292, Asp295, Ile106, Phe8, Gln110, Phe112, Gln127, Phe294
hydroxychloroquine	-5.24	Gln110, Thr111, Thr292, Asp295, Leu202, Phe294, Ile200, Ile249, Gln107, Pro108,Gly109, Asn151, Asn203, Glu240, Pro293
lopinavir	-6.20	Gln110, Asn151, Thr292, Pro293, Gly109, Val104, Ile200, Ile249, Lys102, Arg105, Ile106, Gln107, Pro108, Thr111, Ser158, Asn203, Asp295
nelfinavir	-5.12	Gln110, Thr111, Asn151, Phe294, Val104, Ile249, Pro293, Phe8, Lys102, Arg105, Ile106, Gln107, Phe112, Gln127, Asp153, Ser158, Leu202, Thr292, Asp295
remdesivir	-4.15	Arg105, Gln110, Val104, Ile106, Ile249, Phe294, Gln107, Pro108, Gly109, Thr111, Leu202, Asn203, His246, Thr292, Pro293
		5r82
1	-8.51	Arg298, Val303, Met6, Pro9, Ile152, Phe8, Ala7, Gln127, Asp153, Tyr154, Phe291, Asp295, Gln299, Gly302, Thr304
2	-8.87	Arg298, Val303, Phe8, Met6, Ile152, Ala7, Pro9, Gln127, Asp153, Tyr154, Asp295, Gln299, Gly302, Thr304
3	-7.89	Met6, Asp295, Lys5, Phe8, Phe291, Arg298, Pro9, Gln127, Glu290, Gln299, Gly302, Val303, Thr304
favipiravir	-5.29	Met6, Glu290, Asp295, Gln299, Arg298, Phe3, Arg4, Lys5, Phe8, Thr111, Gln127, Phe291, Thr292, Val296
hydroxychloroquine	-5.17	Met6, Asp295, Phe8, Gly302, Ala7, Pro9, Gln127, Phe294, Arg298, Gln299, Val303, Thr304
lopinavir	-3.89	Arg298, Asp153, Val104, Ile106, Lys102, Gln107, Gln110, Thr111, Asn151, Ser158, Thr292, Phe294, Asp295, Val297, Val303
nelfinavir	-7.85	Glu166, Pro168, Arg188, Gln189, Met165, Phe140, Leu141, Asn142, Ser144, Cys145, His163, Leu167, Thr169, Gly170, Thr190, Gln192
remdesivir	-6.02	Cys44, Thr45, Ser46, Gly143, Cys145, Gln189, Leu167, Glu166, Met49, His41, Thr25, Leu27, Asp48, Leu141, Asn142, Ser144, Pro168, Gly170, Arg188, Thr190, Gln192

* Binding Affinity in kcal/mol.

The high compatibility between the molecular docking calculations and the experimental results have recently enabled these procedures as an essential tool in drug design studies [45]. This method provides useful data regarding to possible bioactivity of the molecules depending on certain biological macromolecules. While the molecular docking methods give information about the activity mechanism of possible drug molecules, they also give numerical values about the interactions [46].

SARS CoV-2 is caused by a coronavirus, which is a single-stranded RNA virus [47]. Anti-SARS CoV-2 therapeutics can target any of several major steps in the viral life cycle, such as virus−cell interactions, virus entry, intracellular viral replication, virus assembly [48]. One of the most important enzymes in the regulation of intracellular replication of the coronavirus is SARS coronavirus main peptidase, and inhibition of this enzyme is important for interrupting the life cycle of the virus [37]. Therefore, the interactions between the molecules in this study and SARS coronavirus main peptidase were investigated and compared to the that of some known antiviral drugs. It was determined with molecular docking

studies that both synthesized molecules and antivirals interacted with the same region of the enzyme. It was recorded that **1**, **2**, and **3** performed H-bonds with Gln110, Asn203 and Thr292. **1** also has pi-sigma interaction with Phe294, and pi-alkyl interactions with Leu202, Ile249 and Pro252. Van der Waals interactions also contributed to -6.25 kcal/mol binding energy calculated for **1**. The contributions to the binding energy, which was calculated as -6.36 kcal/mol for **2**, were recorded as H-bonds with Gln110, Asn203, pi-pi stacked with Phe294 and pi-alkyl interactions with Ile200, Leu202, His246, and also several Van der Waals interactions. The calculated binding energy for **3** was calculated as -6.16 kcal/mol, and similar interactions and many Van der Waals

interactions were detected (Table 2 and Figure 2). Salim and Noureddine investigated the interaction of reference inhibitor AZP (PubChem Code: 5287723) against SARS coronavirus main peptidase by molecular docking and determined the binding constant as -7.499 kcal/mol and this value is higher than the binding constant values of the molecules analyzed in this study [49]. They also examined interactions with some well-known antivirals and determined the binding constants for remdesivir, favipiravir, and hydroxychloroquine as -7.079 kcal/mol, -4.122 kcal/mol, -5.515 kcal/mol, respectively. The results achieved in this study are compared to the previously recorded ones, it is expected that the benzimidazole derivative molecules could provide better inhibitor activity.
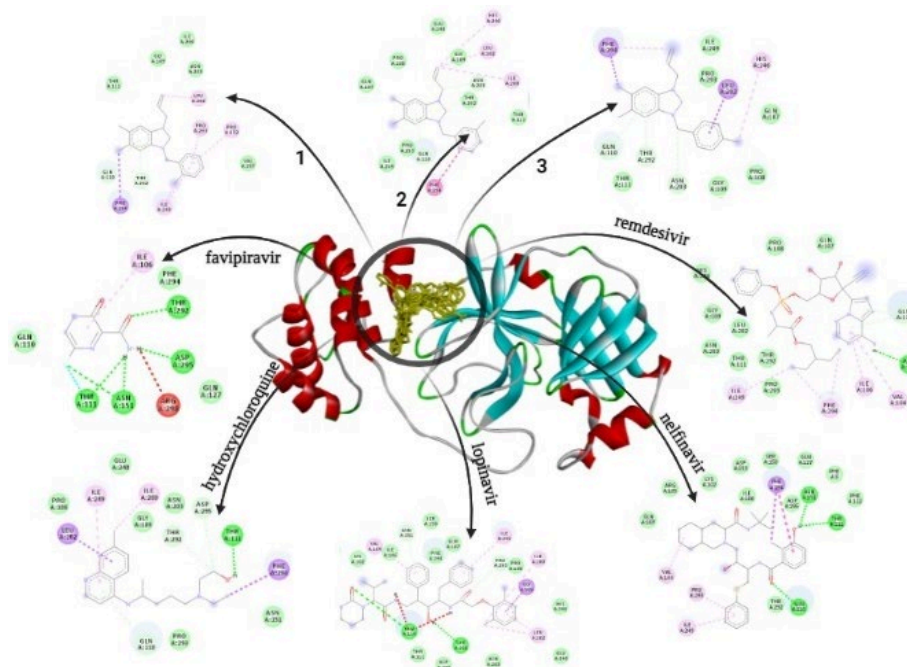

Fig. 2. Molecular docking interactions of SARS coronavirus main peptidase (pdb id:2gtb) with **1, 2, 3,** favipiravir, hydroxychloroquine, lopinavir, nelfinavir, remdesivir.
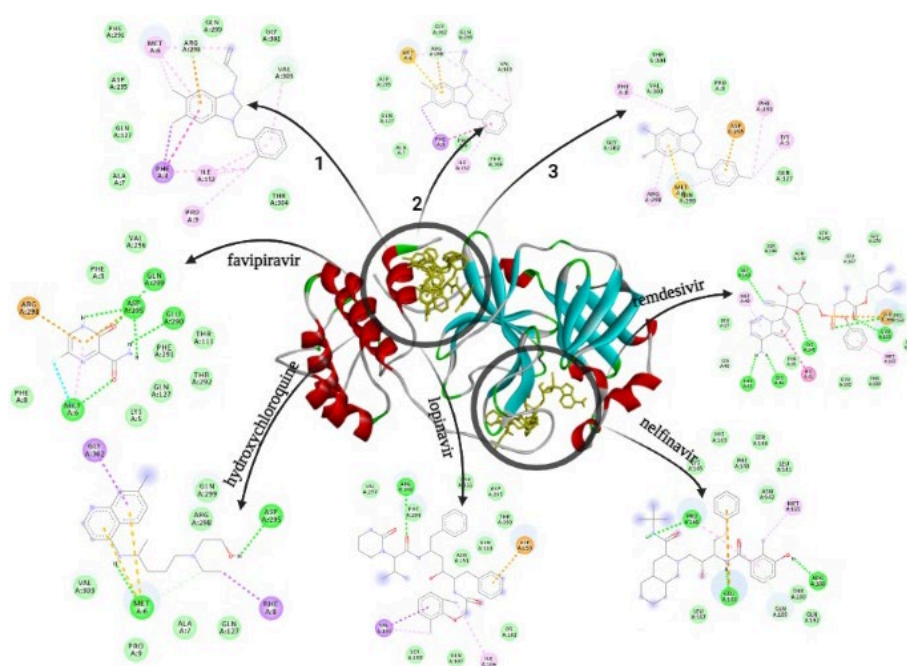

Fig. 3. Molecular docking interactions of COVID-19 main protease (pdb id:5r82) with **1, 2, 3,** favipiravir, hydroxychloroquine, lopinavir, nelfinavir, remdesivir.

One of the enzymes that encodes coronavirus polyproteins is the COVID-19 main protease [50]. These enzymes are frequently used in drug discovery studies since the inhibition of main protease enzyme can prevent the replication of the virus [51]. It was determined that all synthesized molecules interacted with the same region of the target enzyme. This interaction residue is the same for favipiravir, hydroxychloroquine, lopinavir, but different for nelfinavir, remdesivir. Each benzimidazole type molecule gave two H-bond interactions. While H-bonds were formed with Arg298 and Val303 for **1** and **2**, it was noted that Met6 and Asp295 were used for **3**. Both **1** and **2** have also pi-sigma interaction with Phe8. The binding constants calculated for **1**, **2**, and **3** were -8.51 kcal/mol, -8.87 kcal/mol and -7.89 kcal/mol, respectively. The contribution of Van der Waals interactions to the binding scores of molecules is also remarkable (Table 2 and Figure 3). Al-Zahrani were docked several phytochemicals, reference inhibitor (RZS, 6-(ethylamino)pyridine-3-carbonitrile), anti-viral drugs against COVID-19 main protease and the binding constants were recorded −4.90 kcal/mol for RZS, −8.40 kcal/mol for lopinavir, and −7.90 kcal/mol for nelfinavir. 1, 2, and 3 have better binding energy than RZS and nelfinavir but lopinavir better than these molecules [52]. On the other hand, we calculated smaller binding scores for favipiravir, hydroxychloroquine, lopinavir, nelfinavir, and remdesivir for this study and all the benzimidazole type 1, 2, and 3 have higher binding scores than all the well-known anti-viral drugs.

4. Conclusions

NHCs are strong sigma-donor and weak pi-acceptor molecules. The benzimidazole which is one of the important NHCs, generally used as a main scaffold for the development of biological and pharmaceutical active molecule. COVID-19 pandemic still continues, and temporary effects and worldwide availability of vaccination are the main problem against a real victory. An anti-viral drug must be discovered. In this study, new benzimidazole derivative molecules were synthesized and fully characterized. DFT-based calculation methods were used for optimization. HOMO and LUMO were analyzed, and Global Reactivity Descriptors of the molecules were carried out by Koopmans Theorem. Also, the interactions of the molecules were evaluated with COVID-19 main protease, and SARS coronavirus main peptidase and the results were compared with the results of well-known anti-viral (favipiravir, hydroxychloroquine, lopinavir, nelfinavir, remdesivir) by molecular docking methods. As a result of DFT-based theoretical calculations, it was concluded that **1** has stronger reactivity in the reaction medium. The binding energies calculated by molecular docking methods show that these new benzimidazole derivatives could have better inhibition effect than the studied known antiviral drugs on the selected enzymes. Considering the ongoing pandemic conditions, the anti-COVID properties of much more molecules must be investigated for the achievement of the most effective molecule.

Author Contributions

All authors contributed to the study conception and design. Material preparation, data collection and analysis were performed Neslihan Şahin, and Elvan Üstün. The first draft of the manuscript was written by Elvan Üstün and all authors commented on previous versions of the manuscript.

All authors read and approved the final manuscript.

References and Notes

[1]   Crudden, C. M.; Allen, D. P. *Coord. Chem. Rev.* **2004**, *248*, 2247. **[Crossref]**

[2]   Benhamou, L.; Chardon, E.; Lavigne, G.; Bellemin-Laponnaz, S.; Cesar, V. *Chem. Rev.* **2011**, *111*, 2705. **[Crossref]**

[3]   Arduengo III, A. J.; Harlow, R. L.; Kline, M. *J. Am. Chem. Soc.* **1991**, *113*, 361. **[Crossref]**

[4]   Şahin, N.; Üstün, E.; Tutar, U.; Çelik, C.; Gürbüz, N.; Özdemir, İ. *J. Organomet. Chem*. **2021**, *954-955*, 122082. **[Crossref]**

[5]   Serdaroğlu, G.; Şahin, N. *J. Mol. Struct.* **2019**, *1178*, 212. **[Crossref]**

[6]   Helgert, T. R.; Hollis, T. K.; Oliver, A. G.; Valle, H. U.; Wu, Y.; Webster, C. E. *Organometallics* **2014**, *33*, 952. **[Crossref]**

[7]   Yadav, G.; Ganguly, S. *Eur. J. Med. Chem*. **2015**, *97*, 419. **[Crossref]**

[8]   Alamgir, M.; Black, D. S. C.; Kumar, N. In: Bioactive Heterocycles III. Khan, M. T. H., ed. Berlin, Heidelberg: Springer, 2007, p. 87.

[9]   Sharma, S.; Abuzar, S. *Prog Drug Res*. **1983**, 27, 85. **[Crossref]**

[10]   Gaba, M.; Mohan, C. *Med. Chem. Res.* **2016**, *25*, 173. **[Crossref]**

[11]   Barot, P.; Nikolova, K.; Ivanov, S.; Ghate, M. *Mini Rev. Med. Chem.* **2013**, *13*, 1421.

[12]   Arulmurugan, S.; Kavitha, H.; Sathishkumar, S.; Arulmozhi, R. *Mini Rev. Org. Chem.* **2015**, *12*, 178.

[13]   Vasava, M. S.; Bhoi, M. N.; Rathwa, S. K.; Jethava, D. J.; Acharya, P. T.; Patel, D. B.; Patel, H. D. *Mini Rev. Med. Chem.* **2020**, *20*, 532.

[14]   El Rashedy, A. A.; Aboul-Enein, H. Y. *Mini Rev. Med. Chem.* **2013**, *13*, 399.

[15]   Available from: **https://covid19.who.int/**

[16]   Chard, A. N.; Gacic-Dobo, M.; Diallo, M. S.; Sodha, S. V.; Wallace, A. S. *MMWR* **2020**, *69*, 1706. **[Crossref]**

[17]   Muhoza, P.; Danovaro-Holliday, M. C.; Diallo, M. S.; Murphy, P.; Sodha, S. V.; Requejo, J. H.; Wallace, A. S. *MMWR* **2021**, *70*, 1495. **[Crossref]**

[18]   Tarighi, P.; Eftekhari, S.; Chizari, M.; Sabernavaei, M.; Jafari, D.; Mirzabeigi, P. *Eur. J. Pharmacol.* **2021**, *895*, 173890. **[Crossref]**

[19]   Lamontagne, F.; Agoritsas, T.; Siemieniuk, R.; Rochwerg, B.; Bartoszko, J.; Askie, L.; Jacobs, M. *BMJ.* **2021**, 372, 1. **[Crossref]**

[20]   Li, D.; Hu, J.; Li, D.; Yang, W.; Yin, S. F.; Qiu, R. *Top. Curr. Chem.* **2021**, *379*, 1. **[Crossref]**

[21]   Alhazmi, H. A.; Najmi, A.; Javed, S. A.; Sultana, S.; Al Bratty, M.; Makeen, H. A.; Khalid, A. *Front. Immunol.* **2021**, *12*, 1721. **[Crossref]**

[22]   Siles-Lucas, M.; González-Miguel, J.; Geller, R.; Sanjuan, R.; Pérez-Arévalo, J.; Martínez-Moreno, Á. *Trends Parasitol.* **2021**, *37*, 11. **[Crossref]**

[23]   Miller, J. A.; Sivaramakrishnan, R.; Tao, Y.; Goldsmith, C. F.; Burke, M. P.; Jasper, A. W.; Zádor, J. *Prog. Energy Combust. Sci.* **2021**, *83*, 100886. **[Crossref]**

[24] Serdaroğlu, G.; Uludağ, N.; Ercag, E.; Sugumar, P.; Rajkumar, P. *J. Mol. Liq.* **2021**, *330*, 115651. **[Crossref]**

[25] Erdoğan, M.; Serdaroğlu, G. *ChemistrySelect* **2021**, *6*, 9369-9381. **[Crossref]**

[26] Missioui, M.; Mortada, S.; Guerrab, W.; Serdaroğlu, G.; Kaya, S.; Mague, J. T.; Ramli, Y. *J. Mol. Struct.* **2021**, *1239*, 130484. **[Crossref]**

[27] Üstün, E.; Şahin, N.; Çelik, C.; Tutar, U.; Özdemir, N.; Gürbüz, N.; Özdemir, İ. *Dalton Trans.* **2021**, *50*, 15400. **[Crossref]**

[28] Neese, F. *Wiley Interdiscip. Rev. Comput. Mol. Sci.* **2021**, *2*, 73. **[Crossref]**

[29] Neese, F. *Wiley Interdiscip. Rev. Comput. Mol. Sci.* **2018**, *8*, e1327. **[Crossref]**

[30] Becke, A. D. *Phys Rev A.* **1988**, *38*, 3098. **[Crossref]**

[31] Perdew, J.P.; Burke, K.; Ernzerhof, M. *Phys. Rev. Lett.* **1996**, *77*, 3865. **[Crossref]**

[32] Goerigk, L.; Grimme, S. *Phys. Chem. Chem. Phys.* **2011**, *13*, 6670. **[Crossref]**

[33] Van Lenthe, E. V.; Snijders, J. G.; Baerends, E. J. *J. Chem. Phys.* **1996**, *105*, 6505. **[Crossref]**

[34] Koopmans, T. *Physica* **1934**, *1*, 104. **[Crossref]**

[35] Tsuneda, T.; Song, J. W.; Suzuki, S.; Hirao, K. *J. Chem. Phys.* **2010**, *133*, 174101. **[Crossref]**

[36] Available from: **https://autodock.scripps.edu/**

[37] Lee, T. W.; Cherney, M. M.; Liu, J.; James, K. E.; Powers, J. C.; Eltis, L. D.; James, M. N. *J. Mol. Biol.* **2007**, *366*, 916. **[Crossref]**

[38] Douangamath, A.; Fearon, D.; Gehrtz, P.; Krojer, T.; Lukacik, P.; Owen, C. D.;.Walsh, M. A. *Nat. Commun.* **2020**, *11*, 1. **[Crossref]**

[39] Trott, O.; Olson, A. J. *J. Comput. Chem.* **2010**, *31*, 455. **[Crossref]**

[40] Available from: **https://discover.3ds.com/discovery-studio-visualizer-download**

[41] Martin, Y. C. *J. Med. Chem.* **1981**, *24*, 229. **[Crossref]**

[42] Choudhary, N.; Bee, S.; Gupta, A.; Tandon, P. *Comput. Theor. Chem.* **2013**, *1016*, 8. **[Crossref]**

[43] Chattaraj, P. K.; Poddar, A. *J. Phys. Chem. A* **1999**, *103*, 8691. **[Crossref]**

[44] Chattaraj, P. K.; Roy, D. R. *Chem. Rev.* **2007**, *107*, PR46. **[Crossref]**

[45] Nadendla, R. R. *Resonance* **2004**, *9*, 51. **[Crossref]**

[46] De Ruyck, J.; Brysbaert, G.; Blossey, R.; Lensink, M. F. *Adv. Appl. Bioinform. Chem.* **2016**, *9*, 1. **[Crossref]**

[47] Egloff, M. P.; Ferron, F.; Campanacci, V.; Longhi, S.; Rancurel, C.; Dutartre, H.;.Canard, B. *Proc. Natl. Acad. Sci.* **2004**, *101*, 3792. **[Crossref]**

[48] V'kovski, P.; Kratzel, A.; Steiner, S.; Stalder, H.; Thiel, V. *Nat. Rev. Microbiol.* **2021**, *19*, 155. **[Crossref]**

[49] Bouchentouf, S.; Missoum, N. *ChemRxiv* **2020**. **[Crossref]**

[50] Kandeel, M.; Al-Nazawi, M. *Life Sci.* **2020**, *251*, 117627. **[Crossref]**

[51] Kumar, A.; Choudhir, G.; Shukla, S. K.; Sharma, M.; Tyagi, P.; Bhushan, A.; Rathore, M. *J. Biomol. Struct. Dyn.* **2021**, *39*, 3760. **[Crossref]**

[52] Al-Zahrani, A. A. *Nat. Prod. Commun.* **2020**, *15*, 1. **[Crossref]**

How to cite this article